The signaling proteins GPR158 and RGS7 modulate excitability of L2/3 pyramidal neurons and control A-type potassium channel in the prelimbic cortex

Received for publication, January 12, 2019, and in revised form, July 11, 2019 Published, Papers in Press, July 16, 2019, DOI 10.1074/jbc.RA119.007533

Chenghui Song[1], **Cesare Orlandi, Laurie P. Sutton, and Kirill A. Martemyanov**[2]

From the Department of Neuroscience, The Scripps Research Institute, Jupiter, Florida 33458

Edited by Roger J. Colbran

Stress profoundly affects physiological properties of neurons across brain circuits and thereby increases the risk for depression. However, the molecular and cellular mechanisms mediating these effects are poorly understood. In this study, we report that chronic physical restraint stress in mice decreases excitability specifically in layer 2/3 of pyramidal neurons within the prelimbic subarea of the prefrontal cortex (PFC) accompanied by the induction of depressive-like behavioral states. We found that a complex between G protein–coupled receptor (GPCR) 158 (GPR158) and regulator of G protein signaling 7 (RGS7), a regulatory GPCR signaling node recently discovered to be a key modulator of affective behaviors, plays a key role in controlling stress-induced changes in excitability in this neuronal population. Deletion of GPR158 or RGS7 enhanced excitability of layer 2/3 PFC neurons and prevented the impact of stress. Investigation of the underlying molecular mechanisms revealed that the A-type potassium channel Kv4.2 subunit is a molecular target of the GPR158–RGS7 complex. We further report that GPR158 physically associates with Kv4.2 channel and promotes its function by suppressing inhibitory modulation by cAMP–protein kinase A (PKA)–mediated phosphorylation. Taken together, our observations reveal a critical mechanism that adjusts neuronal excitability in L2/3 pyramidal neurons of the PFC and may thereby modulate the effects of stress on depression.

Maladaptive chronic stress impairs appropriate neuronal response to incoming stimuli, resulting in pathological behaviors such as depression. At the cellular level, it involves abnormal changes in structural and functional properties of the neurons in key brain circuits that control mood. For instance, chronic stress significantly reduces the length of apical dendrites and the density of dendritic spines in the prelimbic subregion of the medial prefrontal cortex (mPFC)[3] (1–3). In addition, chronic stress alters electrophysiological properties of the neurons in prelimbic cortex (4), amygdala (5), and nucleus accumbens (6).

Studies in animal models indicate that one of the key physiological parameters impacted by stress is the hypoexcitability of mPFC neurons (7–9). Consistent with these observations, clinically depressed humans also feature a prominent reduction in neuronal activity within dorsolateral PFC (10–12), a region functionally corresponding to rodent mPFC (13, 14). Conversely, optogenetic stimulation (10) or pharmacological activation (15) of mPFC neurons in mice exerted a potent antidepressant-like effect, suggesting that increasing the excitability of mPFC neurons has positive effects on mood and might be exploited for the treatment of depression. Evidence suggests that layer 2/3 (L2/3) neurons of mPFC are particularly vulnerable to stress-induced depression. For instance, induction of the transcription factor ΔFosB in L2/3 of mPFC mediates stress resilience and antidepressant responses (16–18), and deletion of *Wfs1* gene from these neurons impairs the ability of mPFC to suppress stress-induced depressive behaviors (19).

There has been significant progress in understanding the molecular factors and mediators of physiological changes impacting depression-related behaviors acting in various brain regions. A significant role has been shown for the second messenger cAMP. Notably, low cAMP levels have been detected in post-mortem brains of depressed suicide victims (20, 21). In contrast, most effective antidepressants are known to enhance cAMP signaling (22–24). Furthermore, chemogenetic elevation of cAMP levels by designer receptors exclusively activated by designer drugs (DREADDs) can reverse depressive-like behaviors induced by stress (25). In addition to cAMP, inhibitory K^+-conducting channels have also been implicated in the process with significant diversity of types and brain regions involved. It has been shown that prolonged social isolation induces anxiety- and anhedonia-like symptoms, with reduced intrinsic excitability mediated by inward rectifier K^+ and A-type potassium channels (6). Chronic mild stress was also shown to increase the expression of K-ATP channel subunits Kir6.1 and Kir6.2 (26) as well as voltage-gated channel Kv2.1 (27). However, molecular mechanisms and signaling reactions

This work was supported by National Institutes of Health Grants MH105482 and DA026405 (to K. A. M.). The authors declare that they have no conflicts of interest with the contents of this article. The content is solely the responsibility of the authors and does not necessarily represent the official views of the National Institutes of Health.

[1] Present address: Dept. of Neurobiology, University of Alabama, Birmingham, AL 35294.

[2] To whom correspondence should be addressed. Tel.: 561-228-2770; E-mail: kirill@scripps.edu.

[3] The abbreviations used are: mPFC, medial prefrontal cortex; PFC, prefrontal cortex; L2/3, layer 2/3; GPCR, G protein–coupled receptor; GPR158, G protein–coupled receptor 158; RGS7, regulator of G protein signaling 7; PKA, protein kinase A; PRS, physical restraint stress; FST, forced swim test; AP, action potential; RMP, resting membrane potential; ANOVA, analysis of variance; L5, layer 5; HCN, hyperpolarization-activated cyclic nucleotide–gated; KO, knockout; aCSF, artificial cerebrospinal fluid; R_N, input resistance; HEK, human embryonic kidney.

that underlie changes in the excitability of layer 2/3 PFC neurons in depressive states are unknown.

G protein–coupled receptors (GPCRs) mediate the effects of neuromodulators and play key roles in controlling neural activity and excitability (28, 29). In fact, their actions are critically involved in mood regulation, and several GPCRs have been directly and indirectly targeted by existing mainstream and emerging antidepressant medications (30–32). However, current GPCR interventions are limited in efficacy, requiring prolonged administration to exert effects, with nearly half of patients being refractory to the treatment. In this light, significant attention has been focused on poorly explored "orphan" GPCRs for their promise as drug targets for developing more efficacious and precise treatments for depression (33, 34).

We have recently reported the links of the orphan receptor GPR158 to depression. The levels of GPR158 are significantly elevated in human subjects with major depressive disorder and in chronically stressed mice, whereas knockout of GPR158 in mice produces an antidepressant phenotype and stress resilience (35). Interestingly, GPR158 is enriched in L2/3 neurons of mPFC where it is involved in controlling cAMP via an unusual mechanism involving an association with the negative regulator of GPCR signaling, regulator of G protein signaling 7 (RGS7) (35–37). Despite this intriguing initial discovery, the downstream effectors of GPR158 and its role in modulating neuronal activity are not well-understood.

In this study, we report that GPR158 specifically regulates the intrinsic excitability of layer 2/3 pyramidal neurons of mPFC and that this regulation involves its association with RGS7. We further identified Kv4.2 as a major effector regulated by the GPR158–RGS7 complex, physically associated with each other to control A-type K^+ currents in layer 2/3 PFC neurons via a cAMP-dependent mechanism. This establishes a key downstream signaling mechanism by which the antidepressant target GPR158 modulates neuronal function.

Results

Induction of depressive-like behaviors by stress is accompanied by selective reduction in intrinsic excitability of L2/3 prelimbic neurons

We began our studies by examining the effects of stress on the intrinsic excitability of L2/3 neurons in the prelimbic area of the mPFC. Following physical restraint stress (PRS), the depression-like behavior of mice was evaluated in a forced swim test (FST), and whole-cell patch-clamp recordings were obtained from the L2/3 pyramidal neurons (Fig. 1, *A* and *B*). The cell identity was confirmed by action potential (AP) properties and input–output relationship (38, 39). Analysis of the behavioral data indicated that mice subjected to PRS displayed significantly increased immobility during the FST compared with control mice ($t(6) = 6.97$, $p = 0.0004$), demonstrating a depressant-like effect (Fig. 1*C*). Whole-cell recordings revealed a significant ($t(22) = 2.17$, $p = 0.041$) hyperpolarization of the resting membrane potential (RMP) in mice subjected to PRS relative to control subjects (Fig. 1*D*). Interestingly, the excitability of L2/3 pyramidal neurons was also significantly reduced in PRS-exposed mice, as evidenced by fewer action potentials in response to depolarizing current steps compared with control neurons, when the cells were held at their resting potentials (Fig. 1, *E* and *F*). A repeated-measures analysis of variance (ANOVA) revealed significant main effects of group ($F(1,22) = 5.55$, $p = 0.028$) and current intensity ($F(1.4, 30.5) = 223$, $p < 0.001$; Greenhouse–Geisser-corrected). There was also a significant interaction of group with current density ($F(1.4, 30.5) = 3.88$, $p = 0.045$; Greenhouse–Geisser-corrected). Post hoc analysis using *t* test revealed a significant group effect when depolarizing current steps were ≥200 pA (all values, $p < 0.05$). The observed modulation of intrinsic excitability by stress was specific to L2/3 neurons (Fig. 1*G*), as the excitability of layer 5 (L5) neurons obtained from stressed animals was comparable with those from control unstressed mice ($F(1,14) = 0.57$, $p = 0.46$ for main effect of group and $F(2, 112) = 1.6$, $p = 0.22$ for interaction; repeated-measures ANOVA). Taken together, these data suggest that chronic stress induces specific reduction in excitability of L2/3 pyramidal neurons in prelimbic cortex in parallel with development of depressive-like behaviors.

Stress-induced changes in excitability of L2/3 neurons of mPFC are mediated by GPR158–RGS7 complex

In search for the molecular mechanisms underlying changes in intrinsic excitability, we focused on probing the involvement of a GPR158–RGS7 complex, which is prominently enriched in L2/3 neurons as knockout of either GPR158 or RGS7 results in a marked antidepressant phenotype and resilience to stress (35). To exclude the impact of changes in RMP, in the following experiments all cells were held at −70 mV unless noted otherwise. Indeed, elimination of GPR158 or RGS7 significantly increased the intrinsic excitability of layer L2/3 mPFC neurons (Fig. 2). Specifically, $Gpr158^{-/-}$ neurons fired more spikes as compared with littermate control $Gpr158^{+/+}$ neurons (Fig. 2*A*). A repeated-measures ANOVA revealed significant main effects of group ($F(1,23) = 8.77$, $p = 0.007$) and current intensity ($F(1.4, 31.7) = 540$, $p < 0.001$; Greenhouse–Geisser-corrected). There was also a significant interaction of group by current intensity ($F(1.4,31.7) = 7.6$, $p = 0.005$; Greenhouse–Geisser-corrected). Post hoc analysis revealed a significant group effect when depolarizing current steps were ≥200 pA (all values, $p < 0.01$; *t* test). In addition to enhanced excitability, knockout of GPR158 also induced a significant depolarization of RMP ($t(27) = 2.42$, $p = 0.022$), increase in input resistance ($t(27) = 2.25$, $p = 0.033$), decrease in rheobase current ($t(24) = 2.43$, $p = 0.023$), and decrease in delay to the first spike evoked by depolarizing current injection ($t(23) = 2.99$, $p = 0.007$; Table 1). The effect of RGS7 ablation was quantitatively similar to that of GPR158 loss. Layer 2/3 mPFC neurons of $Rgs7^{-/-}$ also fired more action potentials relative to $Rgs7^{+/+}$ neurons in response to depolarizing current injections, whereas chronic stress did not significantly change the excitability of $Rgs7^{-/-}$ neurons (Fig. 2*B*). A repeated-measures ANOVA revealed significant main effects of group ($F(2,40) = 4.43$, $p = 0.018$) and current intensity ($F(1.5,61.8) = 580.0$, $p < 0.001$; Greenhouse–Geisser-corrected), but not interaction of group by current intensity ($F(3.1,61.8) = 2.5$, $p = 0.066$; Greenhouse–Geisser-corrected). Post hoc analysis revealed that the excitability of $Rgs7^{+/+}$ neurons was significantly different from $Rgs7^{-/-}$ neurons either

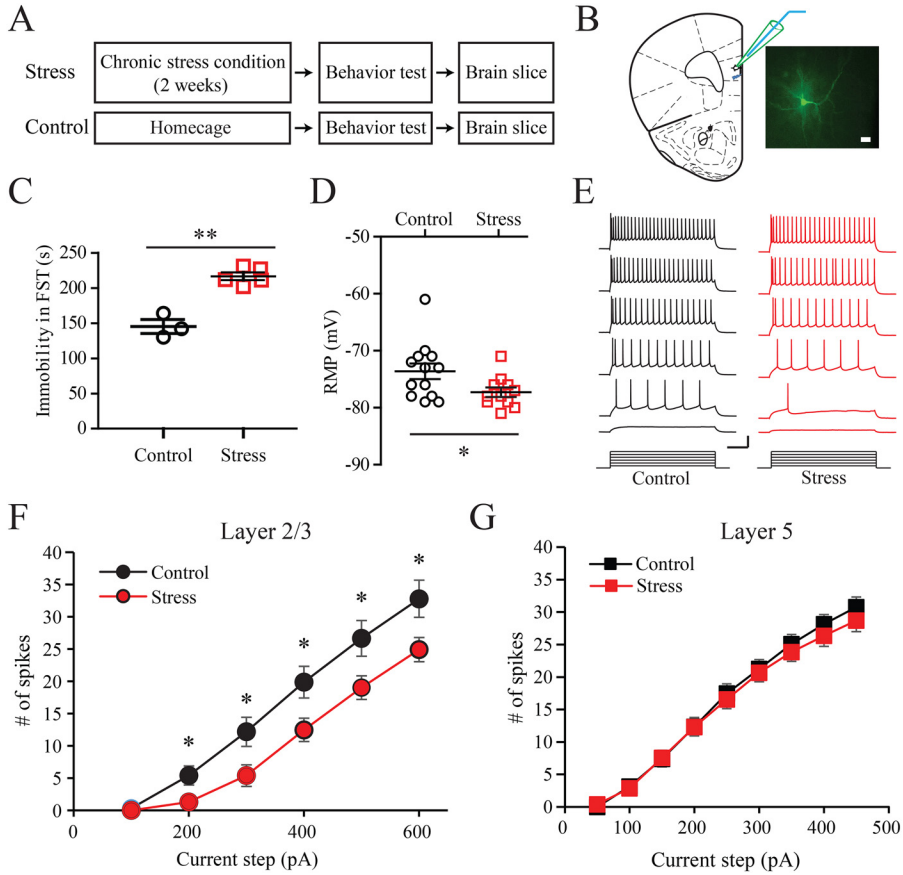

Figure 1. Chronic stress selectively decreases intrinsic excitability of L2/3 prelimbic neurons in mPFC. *A*, experimental design. Mice were either subjected to physical restraint stress for 2 weeks or maintained in their home cages (control group) before behavioral testing. All mice were euthanized, and brain slices were prepared within 1 h following the behavioral evaluation. *B*, schematic diagram of a PFC brain slice and the location of L2/3 pyramidal neurons recorded in this study. *Inset*, a fluorescence microscopy image of representative L2/3 pyramidal cells filled with biocytin during recording and visualized with Alexa Fluor 488. *Scale bar*, 50 μm. *C*, effect of chronic stress on immobility during the FST. Compared with control, stressed mice spent significantly more time immobile during the FST (**, $p < 0.01$ control *versus* stressed mice; Student's *t* test). *D*, effect of chronic stress on the RMP of L2/3 pyramidal neurons in prelimbic cortex ($n = 13$ and $n = 11$ for control and stress, respectively). *E* and *F*, representative traces and average data showing the effect of stress on the excitability of L2/3 pyramidal neurons within mPFC (*, $p < 0.05$ control ($n = 13$) *versus* stressed ($n = 11$) neurons; repeated-measures ANOVA followed by Student's *t* test for each current step). *G*, effect of chronic stress on the excitability of L5 pyramidal cells in prelimbic cortex ($n = 9$ and $n = 7$ for control and stress, respectively). *Error bars* represent S.E.M. values.

with ($p = 0.024$) or without ($p = 0.007$) chronic stress. Furthermore, ablation of RGS7 phenocopied the effects seen upon GPR158 loss, including depolarization of RMP ($t(27) = 2.41$, $p = 0.028$), increase in input resistance ($t(27) = 13.9$, $p = 0.002$), decrease in rheobase current ($t(17) = 2.33$, $p = 0.033$), and decrease in the delay to first spike evoked by depolarizing current injection ($t(17) = 2.38$, $p = 0.029$; Table 1). To test molecular specificity of this effect, we next probed the involvement of R7BP that also prominently regulates RGS7 but does not have an impact on depression-related behaviors (35). We found that elimination of R7BP did not change the intrinsic excitability of L2/3 neurons (Fig. 2*C*). Furthermore, the observed changes following *Gpr158* or *Rgs7* deletion were specific to L2/3 neurons, as no genotype differences were observed in excitability of L5 neurons, with or without stress (Fig. 2, *D*, *E*, and *F*, and Table 2). Together, these data suggest that the GPR158–RGS7 complex specifically modulates intrinsic excitability of layer 2/3 neurons in PFC in response to stress.

GPR158–RGS7 complex exerts its effects on excitability via cAMP

The GPR158–RGS7 complex has been shown to modulate signaling via the second messenger cAMP (37). Thus, we next tested whether the effects of GPR158 and RGS7 on excitability involve changes in cAMP. We found that in WT neurons elevating cAMP by adding the nonhydrolyzable analog S_p-cAMP into the internal recording solution significantly increased intrinsic excitability of layer 2/3 mPFC neurons, mimicking the effect of GPR158 or RGS7 ablation (Fig. 3, *A* and *B*; repeated-measures ANOVA; $F(1,28) = 11.18$, $p = 0.002$). Importantly, elimination of GPR158 completely prevented the effects of S_p-cAMP, which was not observed in *Gpr158*$^{-/-}$ neurons (Fig. 3, *C* and *D*; repeated-measures ANOVA; $F(1,6) = 0.13$, $p = 0.73$). Similarly, S_p-cAMP failed to alter the excitability in neurons lacking RGS7 (Fig. 3, *E* and *F*; repeated-measures ANOVA; $F(1,13) = 1.2$, $p = 0.29$). These data indicate that GPR158 and RGS7 modulate intrinsic excitability of L2/3 prelimbic neurons through regulating intracellular cAMP.

GPR158 and RGS7 modulate A-type potassium channels

The decrease in RMP amid increase in input resistance upon deletion of GPR158 and RGS7 suggests the likely closing of inhibitory ion channels in these neurons as a mechanism for increasing excitability. To establish the identity of such channels, we investigated barium-sensitive potassium current, which includes both inward and outward currents and greatly

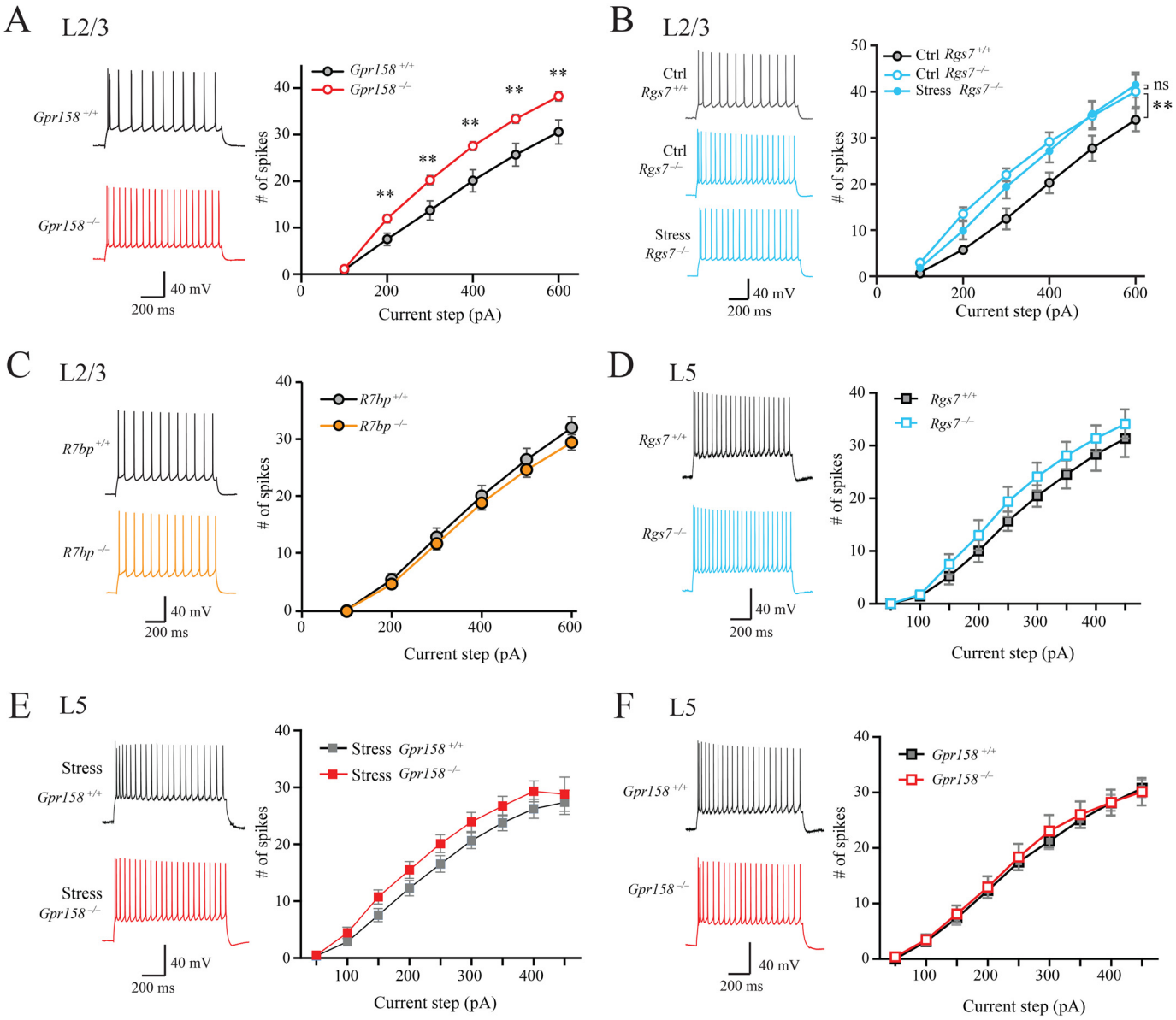

Figure 2. Intrinsic excitability of L2/3 of mPFC neurons is specifically regulated by the GPR158–RGS7 complex. *A*, representative traces and summarized graph showing the effect of genetic knockout of *Gpr158* on the excitability of prelimbic L2/3 pyramidal neurons (**, $p < 0.01$ between genotypes; repeated-measures ANOVA followed by Student's *t* test; $n = 12$ and $n = 13$ for $Gpr158^{+/+}$ and $Gpr158^{-/-}$ neurons, respectively). *B*, representative traces and summary graph showing the effect of genetic knockout of *Rgs7* on the excitability of prelimbic L2/3 pyramidal neurons (**, $p < 0.01$ control $Rgs7^{+/+}$ *versus* control $Rgs7^{-/-}$; *, $p < 0.05$ control $Rgs7^{+/+}$ *versus* stress $Rgs7^{-/-}$; repeated-measures ANOVA followed by least significant difference post hoc tests; $n = 12$, $n = 15$, and $n = 16$ for control $Rgs7^{+/+}$ control, $Rgs7^{-/-}$, and stress $Rgs7^{-/-}$ neurons, respectively). *C*, representative traces and summary graph showing the effect of genetic knockout of *R7bp* on the intrinsic excitability of prelimbic L2/3 neurons ($n = 13$ and $n = 12$ for $R7bp^{+/+}$ and $R7bp^{-/-}$ neurons, respectively). *D*, representative traces and summary graph showing the effect of genetic knockout of *Rgs7* on the intrinsic excitability of prelimbic L5 neurons ($n = 9$ and $n = 8$ for $Rgs7^{+/+}$ $Rgs7^{-/-}$ neurons, respectively). *E*, representative traces and summary graph showing the effect of stress and *Gpr158* knockout on the intrinsic excitability of prelimbic L5 neurons ($n = 23$ and $n = 16$ for $Gpr158^{+/+}$ and $Gpr158^{-/-}$ neurons, respectively). *F*, representative traces and summary graph showing the effect of genetic knockout of *Gpr158* on the intrinsic excitability of prelimbic L5 neurons ($n = 25$ and $n = 19$ for $Gpr158^{+/+}$ and $Gpr158^{-/-}$ neurons, respectively). *Error bars* represent S.E.M. values.

affects membrane properties and excitability (40–42). We found that deletion of GPR158 or RGS7 did not significantly change inward currents when the membrane potential was stepped to a range from −90 to −120 mV (Fig. 4, *A* and *B*). Instead, the outward current was significantly inhibited in the range from −70 to −50 mV (main effects of voltage when tested with repeated-measures ANOVA, $F(1,18) = 9.27$, $p = 0.007$ and $F(1,15) = 7.10$, $p = 0.018$ for *Gpr158* and *Rgs7*, respectively). This difference was also significant when we normalized the barium-sensitive current to a fixed potential at −80 mV (Fig. 4*C*; $t(18) = 3.5$, $p = 0.002$ and $t(15) = 3.0$, $p = 0.009$ for *Gpr158* and *Rgs7*, respectively). These observations suggest the involvement of A-type potassium channels, whose genetic deletion or pharmacological inhibition has been shown to produce effects on depolarizing RMP, input resistant, and firing frequency as well as delaying the first spike in response to depolarizing current injection (43–45), which are similar to changes seen in $Gpr158^{-/-}$ and $Rgs7^{-/-}$ neurons. To test this hypothesis, we directly measured I_A in brain slices using an established protocol (Fig. 5*A*) (46). Indeed, we observed that loss of GPR158

Table 1

Electrophysiological properties of L2/3 pyramidal neurons in prelimbic cortex

Data are means ± S.E. (number of cells). AP amp, action potential amplitude; AP thld, action potential threshold; AP width, action potential halfwidth; mAHP, median afterhyperpolarization. RMPs were measured immediately after whole-cell mode was established by switching to current mode; R_N was the slope of the linear fit of a series of subthreshold currents that did not evoke any active conductance; AP threshold was defined as the voltage when dV/dt first exceeded 28 mV/ms. AP amplitude was measured from threshold. AP width was measured as the width at half of the AP amplitude (from threshold). Delay to 1st spike was the time to the first spike after the stimulus (300-pA current injection) onset. *, statistically different between genotypes, $p < 0.05$; #, statistically different between genotypes, $p < 0.01$. Statistical analysis was performed using two-tailed Student's t test. MΩ, megaohms.

	RMP	R_N	Rheobase	AP thld	AP amp	AP width	mAHP	Delay to 1st spike
	mV	*MΩ*	*pA*	*mV*	*mV*	*μs*	*mV*	*ms*
Gpr158$^{+/+}$	−75.7 ± 1.2 (14)	102.7 ± 8.4 (14)	144 ± 12 (13)	−38.5 ± 1.1 (13)	89.2 ± 1.4 (13)	884 ± 34 (13)	−2.36 ± 0.3 (9)	25.8 ± 2.8 (13)
Gpr158$^{-/-}$	−71.5 ± 1.4 (13)*	130.7 ± 9.2 (13)*	107 ± 7 (11)*	−39.0 ± 1.2 (11)	91.4 ± 1.3 (11)	853 ± 34 (11)	−2.21 ± 0.2 (10)	16.1 ± 0.8 (13)#
Rgs7$^{+/+}$	−76.5 ± 1.5 (10)	84.8 ± 9.5 (9)	148 ± 11 (9)	−41.8 ± 1.3 (9)	89.9 ± 1.0 (9)	865 ± 48 (9)	−1.92 ± 0.2 (9)	31.0 ± 6.3 (9)
Rgs7$^{-/-}$	−70.9 ± 1.4 (10)*	159.2 ± 17.1 (10)#	106 ± 13 (10)*	−38.4 ± 1.2 (10)	91.7 ± 1.3 (10)	898 ± 31 (10)	−2.07 ± 0.1 (9)	17.5 ± 1.7 (10)*
Rgs7BP$^{+/+}$	−73.8 ± 1.4 (15)	86.26 ± 10 (13)	183.0 ± 18 (13)	−37.1 ± 0.9 (13)	89.44 ± 0.7 (13)	873.6 ± 22 (13)	−1.40 ± 0.2 (13)	32.5 ± 4.4 (12)
Rgs7BP$^{-/-}$	−71.5 ± 1.2 (12)	89.31 ± 8.4 (12)	163.3 ± 12 (12)	−37.6 ± 0.6 (12)	90.77 ± 0.9 (12)	993.8 ± 61 (12)	−1.27 ± 0.1 (12)	31.2 ± 3.9 (11)

Table 2

Electrophysiological properties of L5 pyramidal neurons in prelimbic cortex

Data are means ± S.E. (number of cells). AP amp, action potential amplitude; AP thld, action potential threshold; AP width, action potential halfwidth; mAHP, median afterhyperpolarization. RMPs were measured immediately after whole-cell mode was established by switching to current mode; R_N was the slope of the linear fit of a series of subthreshold currents that did not evoke any active conductance; AP threshold was defined as the voltage when dV/dt first exceeded 28 mV/ms. AP amplitude was measured from threshold. AP width was measured as the width at half of the AP amplitude (from threshold). Delay to 1st spike was the time to the first spike after the stimulus (300-pA current injection) onset. MΩ, megaohms.

	RMP	R_N	Rheobase	AP thld	AP amp	AP width	mAHP	Delay to 1st spike
	mV	*MΩ*	*pA*	*mV*	*mV*	*μs*	*mV*	*ms*
Gpr158$^{+/+}$	−62 ± 0.8 (25)	131 ± 12 (25)	114 ± 10 (16)	−35 ± 0.4 (16)	86 ± 1.4 (16)	790 ± 79 (16)	−3.7 ± 0.2 (23)	15.0 ± 1.0 (25)
Gpr158$^{-/-}$	−63 ± 0.8 (19)	139 ± 17 (19)	126 ± 19 (13)	−36 ± 0.9 (12)	84 ± 1.8 (12)	910 ± 91 (12)	−3.7 ± 0.2 (17)	17.7 ± 1.7 (19)
Rgs7$^{+/+}$	−61 ± 1.6 (9)	107 ± 18 (9)	148 ± 18 (9)	−36 ± −36 (9)	88 ± 1.9 (9)	984 ± 98 (9)	−3.9 ± 0.5 (5)	14.8 ± 2.3 (9)
Rgs7$^{-/-}$	−61 ± 1.1 (8)	113 ± 14 (8)	135 ± 16 (8)	−37 ± −37 (8)	88 ± 1.4 (8)	966 ± 96 (8)	−3.4 ± 0.3 (7)	14.1 ± 1.1 (8)

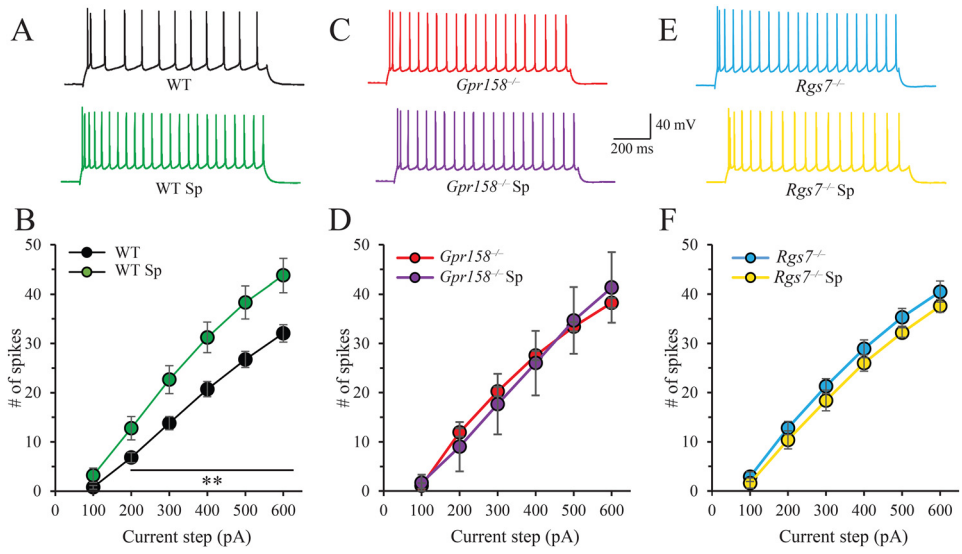

Figure 3. Changes in excitability of L2/3 mPFC neurons upon elimination of GPR158 and RGS7 are mediated by the cAMP signaling. Excitability was compared between neurons recorded with or without S_p-cAMP in the internal solutions. *A* and *B*, representative traces and summary data showing the effect of S_p-cAMP on the intrinsic excitability of WT neurons (**, $p < 0.01$ WT *versus* WT S_p; repeated-measures ANOVA followed by post hoc t test; $n = 21$ and $n = 9$ for WT and WT S_p neurons, respectively). *C* and *D*, representative traces and summarized data showing the effect of S_p-cAMP on the intrinsic excitability of *Gpr158*$^{-/-}$ neurons ($n = 3$ and $n = 5$ for *Gpr158*$^{-/-}$ and *Gpr158*$^{-/-}$ S_p neurons, respectively). *E* and *F*, representative traces and summarized data showing the effect of S_p-cAMP on the intrinsic excitability of *Rgs7*$^{-/-}$ neurons ($n = 10$ and $n = 5$ for *Rgs7*$^{-/-}$ and *Rgs7*$^{-/-}$ S_p neurons, respectively). *Error bars* represent S.E.M. values.

or RGS7 (Fig. 5, *B* and *C*) significantly reduced I_A ($t(16) = 2.41$, $p = 0.029$ for GPR158 and $t(25) = 2.89$, $p = 0.009$ for RGS7. These data support the involvement of A-type potassium channels in modulating membrane properties and intrinsic excitability of L2/3 pyramidal neurons caused by inactivation of GPR158–RGS7 complex.

GPR158 directly modulates Kv.4.2 A-type potassium channel

Kv4.2 potassium subunit is the major contributor of A-type currents (47). Interestingly, proteomic profiling has identified GPR158 to be present among a large number of proteins associated with Kv4.2 potassium channel (48, 49). Thus, we next turned to a transfected HEK293 cell system to specifically test the interaction of GPR158–RGS7 with Kv4.2 and study its functional consequences. Indeed, we found that GPR158 effectively coimmunoprecipitated with Kv4.2 when coexpressed in HEK293 cells (Fig. 6*A*), validating their physical binding. In support of our model, the Kv4.2 channel is prominently modulated by cAMP via PKA-dependent phosphorylation of Thr-38 and Ser-552, which inhibits its plasma membrane traf-

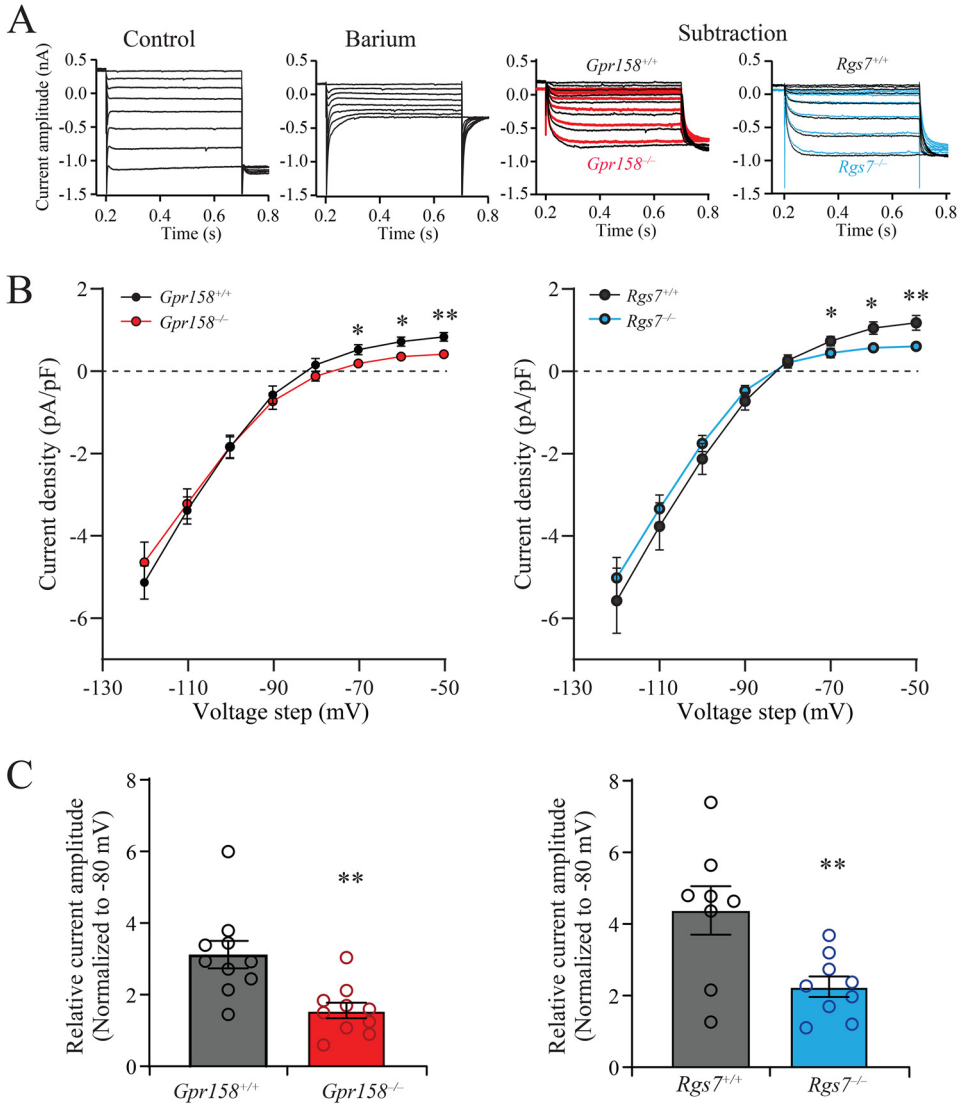

Figure 4. Loss of GPR158 or RGS7 significantly suppresses outward potassium current. *A*, representative traces showing the current response to voltage steps that were recorded before (control) and 10 min after bath application of barium chloride (100 μM). Barium-sensitive current was obtained by subtracting responses of post- from pre-barium chloride application. *B*, summary data showing the effect of genetic knockout of GPR158 (*left*) and RGS7 (*right*) on barium-sensitive current (*, $p < 0.05$; **, $p < 0.01$ between genotypes; repeated-measures ANOVA followed by Student's *t* test; $n = 10$, $n = 10$, $n = 8$, and $n = 9$ for $Gpr158^{+/+}$, $Gpr158^{-/-}$, $Rgs7^{+/+}$, and $Rgs7^{-/-}$ neurons, respectively). *C*, summarized bar graph with individual data points showing the effect of genetic knockout of GPR158 (*left*) and RGS7 (*right*) on relative current amplitude at −50 mV (relative to −80 mV). *pF*, picofarad. *Error bars* represent S.E.M. values.

ficking (50, 51). To investigate the impact of GPR158 on Kv4.2 gating and the relevance of cAMP in this process, we coexpressed GPR158 with WT Kv4.2 or a Kv4.2AA double mutant (Kv4.2 T38A/S552A) that abolishes PKA regulation at the two sites. Cells were further cotransfected with the construct encoding mCherry to identify the cells that express the desired constructs (Fig. 6*B*). Whole-cell patch-clamp recordings revealed that transfecting Kv4.2 resulted in a rapidly activating and inactivating K^+ current typical of I_A, which was absent in untransfected cells (Fig. 6*C*). Mutation of Kv4.2 channels or coexpression of GPR158 might not affect RMP because the current used to hold the cells at −50 mV was comparable between groups (Fig. 6*D*, *left*; $F(3,36) = 1.46$, $p = 0.24$). Furthermore, coexpression of GPR158 did not affect the peak amplitude of the current carried by either WT or mutant Kv4.2 channel (Fig. 6*D*, *right*; $F(3,36) = 0.84$, $p = 0.48$; one-way ANOVA), suggesting the lack of the channel modulation at the baseline when cAMP levels are low (47).

We next studied the effect of GPR158 on Kv4.2 upon elevating cAMP concentration by forskolin treatment, which activates the cAMP-producing enzyme adenylyl cyclase (Fig. 6*E*). Consistent with previously noted inhibitory effects of cAMP, forskolin quickly inhibited the peak amplitude of Kv4.2 current in all groups of cells (main effect of time, $F(3.1,102.7) = 36.4$, $p < 0.001$; repeated-measures ANOVA, Greenhouse–Geisser-corrected). There was also a significant effect of group ($F(3,33) = 7.59$, $p = 0.001$) and group by time interaction ($F(9.3,102.7) = 3.60$, $p = 0.001$). This effect was further underscored by the analysis of the maximal effect size at the effect plateau (Fig. 6*F*); one-way ANOVA ($F(3,33) = 5.57$, $p = 0.003$). The follow-up post hoc tests confirmed the role of cAMP in this effect: the Kv4.2AA mutant was insensitive to cAMP modula-

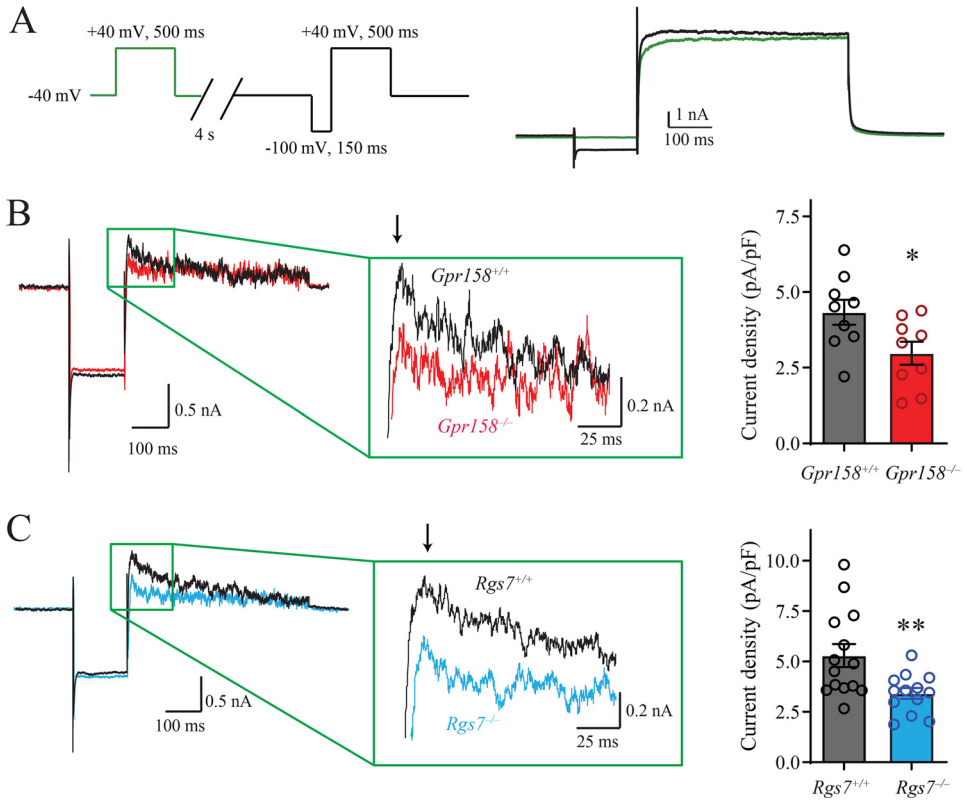

Figure 5. Elimination of GPR158 or RGS7 suppresses A-type potassium current in L2/3 mPFC neurons. *A*, recording protocol used to isolate A-type potassium current (*left*) and representative traces (*right*) showing current response in the absence (*green*) and presence of a −100-mV prepulse (*black*). *B*, representative traces (*left*) and summarized bar graph (*right*) showing the effect of genetic knockout of *Gpr158* on the amplitude of A-type potassium current in L2/3 pyramidal neurons within prelimbic cortex (*, $p < 0.05$ between genotypes; Student's *t* test; $n = 9$ and $n = 9$ for $Gpr158^{+/+}$ and $Gpr158^{-/-}$ neurons, respectively). *C*, representative traces (*left*) and summarized bar graph (*right*) showing the effect of genetic knockout of *Rgs7* on the amplitude of A-type potassium current in L2/3 pyramidal neurons within prelimbic cortex (**, $p < 0.01$ between genotypes; Student's *t* test; $n = 14$ and $n = 13$ for $Rgs7^{+/+}$ and $Rgs7^{-/-}$ neurons, respectively). An *arrow* indicates peak current measured as the amplitude of A-type potassium current. *pF*, picofarad. *Error bars* represent S.E.M. values.

tion, and forskolin was significantly less effective in inhibiting its currents ($p < 0.05$). Similarly, introduction of GPR158 also made Kv4.2 less sensitive to inhibition by forskolin ($p < 0.05$). Finally, addition of GPR158 to Kv4.2AA did not further alter its forskolin inhibition, indicating an occlusion of the effect ($p < 0.05$). It is notable that forskolin also induced a slight reduction of the currents in cells expressing Kv4.2AA constructs. This is likely due to the phosphorylation of the pore-forming subunit mediated by the extracellular signal-regulated kinase/mitogen-activated protein kinase signaling cascade (52, 53). These observations suggest that the GPR158 complexes counteract the inhibitory action of cAMP on A-type conductances via phosphorylation of the PKA-dependent sites on Kv4.2 channels (Fig. 6*G*).

Discussion

The present study demonstrates for the first time that GPR158 and RGS7 regulate intrinsic excitability of pyramidal cells in superficial layers (L2/3) of mPFC. This effect was specific to this cellular population and was not observed in L5 neurons. Neither was it observed in mice lacking R7BP. Our data also indicate that GPR158 and RGS7 regulate the A-type potassium channels of L2/3 neurons in mPFC via cAMP-dependent phosphorylation. Taken together, this study suggests that modulating intrinsic excitability via A-type potassium channels may contribute to the antidepressant-like phenotype observed in GPR158- and RGS7-knockout animals (35, 37).

The current observations are consistent with the critical role of mPFC in regulating behavioral response to stress and the susceptibility to detrimental effects induced by stress (54, 55). In particular, chronic stress has been noted to cause dendritic branch shrinking, spine loss (56, 57), and synaptic modifications (58, 59) in mPFC neurons. Furthermore, deletion of *Wfs1* (gene responsible for Wolfram syndrome) in L2/3 pyramidal cells resulted in neuronal hyperactivation and engagement of the hypothalamic–pituitary–adrenal axis, impairing the suppression of stress-induced depressive behaviors (19). Thus, our findings suggest that the GPR158–RGS7 complex may be a key modulator that gates the excitability of L2/3 mPFC neurons in response to stress and regulates behavioral outcomes.

In this study, we identified a molecular target of GPR158–RGS7 action involved in the modulation of excitability. We show that the GPR158–RGS7 complex modulates the activity of A-type potassium channel Kv4.2 via a cAMP-dependent mechanism. Although GPR158 and RGS7 likely regulate several effectors and affect several processes, our observations suggest that their effects on excitability may be mediated, at least in part, by Kv4.2 channels, which are well-known for their role in regulating neuronal excitability (50, 60). Mechanistically, pre-

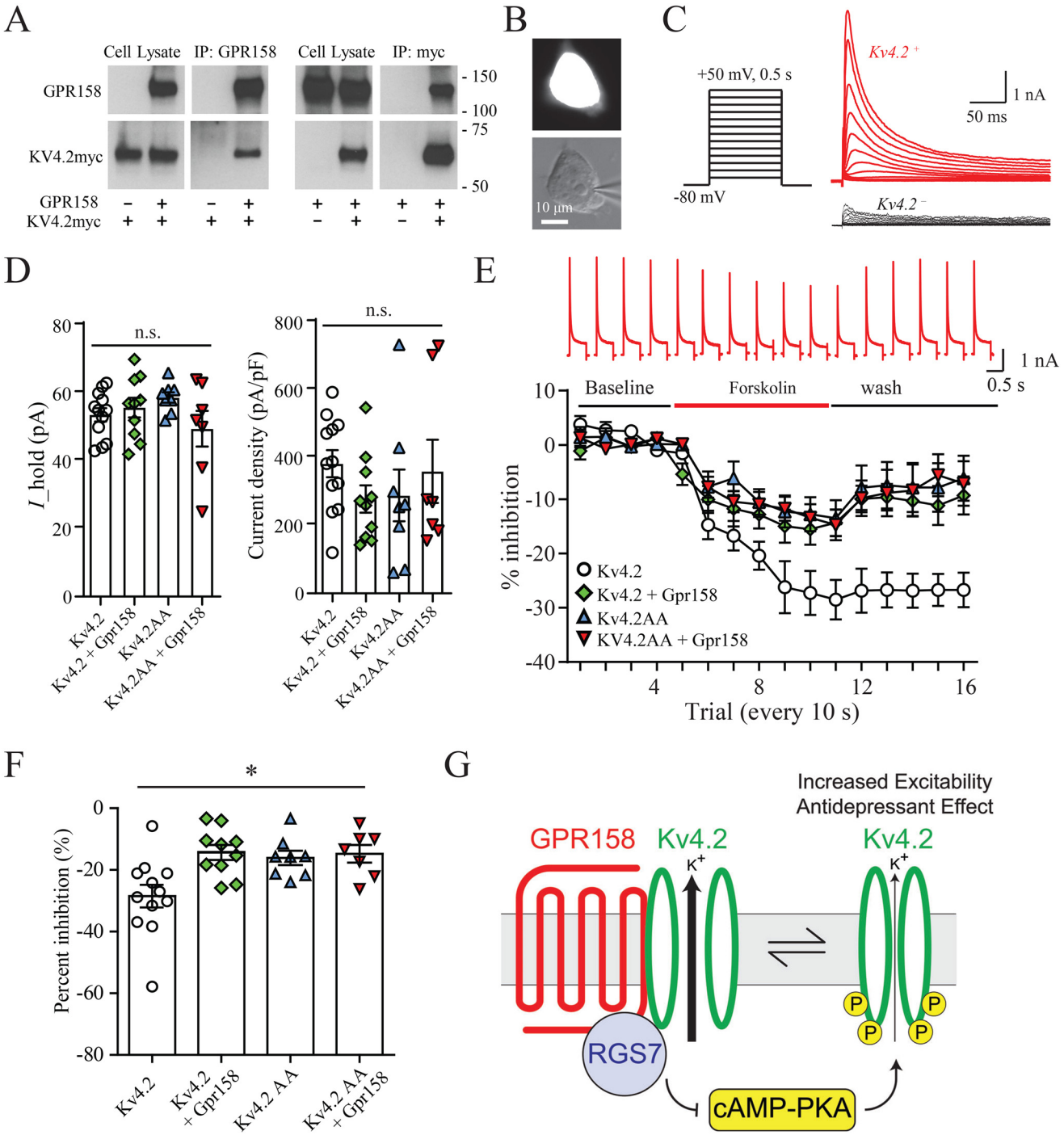

Figure 6. GPR158–RGS7 regulates Kv4.2 channels in a cAMP/PKA-dependent manner. *A*, *in vitro* coimmunoprecipitation of GPR158 with Kv4.2 in HEK293 cells transfected with the indicated constructs. Immunoprecipitated (*IP*) proteins were detected by Western blotting using a specific antibody against GPR158 or an anti-myc antibody to recognize Kv4.2. 1.5% of the cell lysate (input) and 25% of the eluted immunoprecipitation was loaded per well. *B*, representative fluorescence (*top*) and IR differential video interference microscopy (*bottom*) images showing a HEK293 cell that expressed *Gpr158*, Kv4.2 channels, and mCherry. Whole-cell patch-clamp recordings were obtained from fluorescently labeled cells. *C*, recording protocol and representative current responses of HEK293 cells that expressed Kv4.2 channels (*red*) and cells that did not express the channels (*black*). *D*, point mutations in Kv4.2 channels (Kv4.2AA) or coexpression of GPR158 did not significantly affect the current used to hold the cells at −50 mV (*left*) and the peak amplitude of Kv4.2 current in HEK293 cells (*right*). *E*, effect of forskolin on the peak amplitude of Kv4.2 current (***, $p < 0.001$ between Kv4.2 and all other three groups; repeated-measures ANOVA followed by least significant difference post hoc test). *F*, summarized data with individual cells showing the maximal effect of forskolin-induced inhibition on the peak amplitude of Kv4.2 current (trial 11; *, $p < 0.05$ between Kv4.2 and all other three groups; one-way ANOVA followed by Bonferroni's post hoc test). *G*, proposed model for GPR158–RGS7 involvement in modulation of intrinsic excitability. GPR158–RGS7 complex inhibits the production of cAMP, which inhibits potassium current through PKA-dependent phosphorylation of Kv4.2 channels to affect the extent of A-type current generation that reduces excitability. Elimination of GPR158–RGS7 complex would enhance cAMP–PKA activation, which phosphorylates A-type potassium channels, inhibiting them to increase excitability to produce antidepressant effects. *Error bars* represent S.E.M. values.

vious studies have established that the phosphorylation of Kv4.2 channels by cAMP–PKA causes their internalization and thus increases neuronal excitability (44, 50, 51, 61). Because the genetic knockout of *Gpr158* or *Rgs7* also increases intracellular cAMP levels (35, 37), the enhanced excitability in neurons lacking GPR158 or RGS7 is likely due to smaller A-type potassium current mediated by PKA phosphorylation. The identification of A-type potassium channels as the targets for GPR158–RGS7 effects in mPFC neurons was unexpected as our working hypothesis based on prior studies in hippocampal neurons favored a role for G protein–gated inwardly rectifying potassium channels in this process (62). Another channel that could have been involved in this process is hyperpolarization-activated cyclic nucleotide–gated (HCN) that is active at resting membrane potentials and greatly facilitated by cAMP (63, 64). The net effect of activating HCN channels is a decrease in excitability primarily due to reduction in membrane resistance (65, 66). Because cAMP is increased upon the loss of RGS7–GPR158 and the excitability is also increased, we think it is unlikely that HCN channels contribute to RGS7–GPR158-mediated regulation of excitability in L2/3 neurons of mPFC. The expression pattern of HCN channels with prominent presence in hippocampal CA1 (67–69) and deep but not superficial layers (L2/3) of mPFC (39, 70) may provide an explanation for the lack of their involvement. Thus, differential expression of ion channels across brain regions may set up bidirectional effects of GPR158–RGS7 on neuronal excitability in a neuron-selective fashion.

The contribution of Kv4.2 channels to the effects of GPR158–RGS7 complex on depression remains to be fully elucidated. Based on increased inhibition of Kv4.2 observed in the absence of GPR158 or RGS7, one can expect that elimination of Kv4.2 would also result in antidepressant behavior. However, Kv4.2-knockout mice do not exhibit a consistent phenotype when evaluated by depression/anxiety-related tests. One study reported a prodepressant increase in the immobility time in FST but lack of the effect in the tail suspension test (71). A subsequent study failed to confirm the prodepressant phenotype and found that Kv4.2-KO mice behaved similarly to controls in the FST test (72). However, both of the studies reported a mild anxiolytic phenotype (71, 72). Furthermore, Kv4.2-KO mice exhibited an abnormal response to stress diminishing its effects on depression-related behavioral changes (71), whereas increased immobility during FST may also be viewed as a learned habituation and desensitization to stress (73, 74). There are several possible explanations for why the marked antidepressant phenotype associated with GPR158–RGS7 ablation is not recapitulated by Kv4.2 KO. First, loss of the Kv4.2 channels is well-known to be compensated by the up-regulation of other K^+ channels that contribute to A-type conductance (75); thus, constitutive knockout of Kv4.2 may be insufficient for altering excitability to the threshold that triggers behavioral changes. Second, GPR158–RGS7 complex may not be involved in regulating Kv4.2 in all relevant brain circuits. Studies indicate that GPR158–RGS7 action in PFC is sufficient for producing an impact on affective behaviors (35, 37) and so might be Kv4.2. However, in global Kv4.2 KO, this action may be compensated by counteracting effects from other circuits where Kv4.2 may not be regulated in similar fashion by GPR158–RGS7. Testing these possibilities would require examining the effects of manipulations with Kv4.2 in adult mice with region selectivity by either genetic or pharmacological strategies.

Taken together, the current study suggests that changes in the excitability of neurons in superficial layers of mPFC may be a cellular mechanism underlying the antidepressant effect of GPR158 or RGS7 knockout. The GPR158–RGS7 complex may regulate Kv4.2 channels through controlling the cAMP–PKA signaling cascade. This may provide a new therapeutic strategy for treatment of stress-induced depression, by regulation of the excitability of L2/3 neurons in PFC via suppressing the activity of GPR158–RGS7 complex.

Experimental procedures

Animal models

All studies were carried out in accordance with the National Institute of Health guidelines and were granted formal approval by the Institutional Animal Care and Use Committee of The Scripps Research Institute. The generation of *Gpr158*$^{-/-}$ (36, 37), *Rgs7*$^{-/-}$ (76), and *R7bp*$^{-/-}$ (77) mice was described previously. All mice were maintained on C57/Bl6 background and were 2–5 months old during the experiments. All animals used for comparing genotypes were littermates derived from heterozygous breeding pairs. Mice were housed in groups on a 12-h light–dark cycle with food and water available *ad libitum*. Both male and female mice were used in this study.

Genetic constructs

Cloning of full-length mouse GPR158 into the pcDNA3.1/V5-His-TOPO was described previously (78). The plasmid encoding full-length mouse Kv4.2 (GenBank™ accession number NM_019697; myc-DDK-tagged in C terminus) for mammalian expression was purchased (Origene). Kv4.2 bearing mutations to express Ala at the two PKA target sites Thr-38 and Ser-552 (Kv4.2AA) was generated using the In-Fusion HD cloning system (Clontech) in pcDNA3.1. Each construct was verified by DNA sequencing.

Behavior and physical restraint stress

PRS was performed in plastic tubes (30-mm diameter × 115-mm length) with holes for ventilation. Stressed mice were restrained horizontally in tubes for 2 h for 14 days; nonstressed mice were left undisturbed in their home cages. On day 15, all mice underwent an FST that was conducted using a vertical glass cylinder filled with water (25 °C). The mice spent 6 min in the water, and immobility was scored from 2 to 6 min by an independent researcher. A mouse was regarded as immobile when floating motionless or making only those movements necessary to keep its head above the water. Brain slices were prepared within 1 h following the FST, and whole-cell patch-clamp recordings were obtained from pyramidal cells in L2/3 of prelimbic area.

Slice preparation and whole-cell recordings from brain slices

Coronal slices (300 μm) containing prefrontal cortex (anteroposterior +1.5–2.2) were cut in ice-cold aCSF (124 mM

NaCl, 2.8 mM KCl, 1.25 mM NaH_2PO_4, 2 mM $CaCl_2$, 1.25 mM $MgSO_4$, 26 mM $NaHCO_3$, 10 mM glucose, pH 7.5, bubbled with 95% O_2, 5% CO_2) using a vibrating tissue slicer (VT1200, Leica). Slices were transferred to a holding chamber (79) where they remained in oxygenated aCSF at 32–35 °C until use. During recording, slices were transferred to a submerged recording chamber where they were continuously perfused at 2 ml/min with oxygenated aCSF and maintained at 32–36 °C using an inline temperature controller. Neurons were visualized with IR differential video interference microscopy. Whole-cell recordings were obtained with standard-wall borosilicate glass pipettes (2–5 megaohms) filled with the following solution: 110 mM K-gluconate, 20 mM KCl, 10 mM di-Tris-P-creatine, 10 mM HEPES, 2 mM $MgCl_2$, 2 mM Na_2ATP, 0.3 mM Na_2GTP with a pH of 7.3 and osmolarity of 290 mosmol. Prelimbic L2/3 neurons were recognized by their large somata, prominent apical dendrite, and firing properties. To verify identity, some cells were injected with 0.1% biocytin through the recording electrode and visualized using a streptavidin Alexa Flour 488 reaction as described previously (39). One neuron was studied in each slice. Only neurons with an RMP more negative than −60 mV, an input resistance (R_N) >50 megaohms, an AP amplitude >45 mV relative to threshold, and an access resistance less than 20 megaohms were included.

RMP was obtained immediately by switching to current clamp after whole-cell mode was established. The membrane capacitance was estimated by using the auto C-slow function in Patchmaster. Intrinsic properties of mPFC neurons were recorded 3 min later (to allow the diffusion of internal solution) according to the following protocols. 1) *V–I* relationships were obtained from a series of 500-ms current injections (range −300 to 50 pA) and plotting the plateau voltage deflection against current amplitude. Neuronal R_N was determined from the slope of the linear fit portion of the *V–I* plot where the voltage sweeps did not exhibit sags or active conductance (80). 2) AP properties, including the minimum current necessary to elicit an AP ($I_{threshold}$), were studied with an ascending series of 500-ms depolarizing pulses to elicit one single spike. 3) Neuronal excitability was assessed by counting the number of spikes evoked in response to a series of 1-s depolarizing steps (range, 100–600 pA at 100-pA increments or 50–450 pA at 50-pA increases with a 20-s intertrial interval).

To record barium-sensitive current, cells were held at −50 mV and *V–I* relationships were obtained from a serious of voltage steps (from −50 to −120 mV) before and 10 min after bath application of 100 μM barium chloride. Barium-sensitive currents were calculated by subtraction of current responses to voltage steps in the presence and absence of barium. A-type current was isolated using a voltage protocol described previously (46). Briefly, the cells were first held at −40 mV to inactivate most of the outward current. After stabilization, a step was made to + 40 mV for 500 ms and then returned to −40 mV for 5 s followed by a prepulse to −100 mV (150-ms duration) to allow preferential recovery of the A-type current. This prepulse duration is long enough to recover most of the A current but is too short to recover the majority of the delayed rectifier currents (81, 82). A-type current was defined as the difference between the peak current during the test potential (+40 mV) after the prepulse and current during the test pulse without prepulse (relevant to the current used to hold the cells at −40 mV).

Cell culture and whole-cell recording from transfected HEK293 cells

Cell culture was carried out using standard procedures. HEK293T/17 cells were cultured at 37 °C in 5% CO_2 in Dulbecco's modified Eagle's medium supplemented with 10% fetal bovine serum, minimum essential medium nonessential amino acids, 1 mM sodium pyruvate, and 2 mM GlutaMAX. 80,000 cells were plated on 12-mm poly-D-lysine–coated glass coverslips and transfected using Lipofectamine LTX (Invitrogen) and Plus reagent (Invitrogen) with a 1:1 ratio of GPR158 and Kv4.2 expression constructs and used 16 h later. Transfected cells were identified by expression of the fluorescent protein mCherry. Coverslips were bathed in recording solution for electrophysiological recording containing the following: 141 mM NaCl, 4.7 mM KCl, 1.2 mM $MgCl_2$, 1.8 mM $CaCl_2$, 10 mM glucose, 10 mM HEPES, pH 7.4, with NaOH. Whole-cell recordings were performed on fluorescently labeled cells at room temperature with glass pipettes filled with internal solution containing 125 mM KCl, 4 mM $MgCl_2$, 10 mM HEPES, 10 mM EGTA, 5 mM Mg-ATP, pH 7.2, with KOH. Pipette resistance was between 2 and 5 megaohms, and series resistance ranged between 2 and 10. The cells were held at −50 mV when the whole-cell configuration was obtained. The capacitance and series resistance were compensated using the auto function of Patchmaster software before recording the currents. Under voltage clamp, Kv4.2 channel currents were evoked by a brief prepulse to −80 mV followed by pulses of depolarization (Fig. 6*C*, *left*). Kv4.2 currents exhibited rapid activation and inactivation typical of A-type potassium currents, whereas endogenous Kv4.2 currents in HEK cells were relatively negligible; therefore, they were not quantified (Fig. 6*C*, *right*). To study the effect of forskolin on the peak amplitude of Kv4.2 channel current, a test pulse (+40 mV, 500 ms) was given every 10 s, and the peak current of each pulse was measured. After a baseline recording, forskolin (100 μM) was directly applied to the cell with an SF-77B rapid perfusion system (Warner Instruments, Inc., Hamden, CT). Percent inhibition of the peak Kv4.2 current by forskolin was expressed as $(1 - I_{test}/I_{baseline}) \times 100\%$ where I_{test} is the peak current of each test pulse and $I_{baseline}$ is the baseline amplitude (average of four pulses before forskolin application). All chemicals were purchased from Sigma. All data were collected with a HEKA EPC10 amplifier system (HEKA Instruments, Holliston, MA) and transferred to a personal computer using an ITC-16 digital-to-analog converter (HEKA Instruments). The signals were filtered at 2.9 kHz and digitized at 10 kHz using Patchmaster software (HEKA Instruments). Data were analyzed offline using Patchmaster. Voltages were not corrected for the liquid–liquid junction potential.

Immunoprecipitation

Two million HEK293T/17 cells/well were plated in a 6-well culture plate and transfected using Lipofectamine LTX and Plus reagent with a 1:1 ratio of GPR158 and Kv4.2myc plasmids. Cells were harvested 24 h later and lysed in 500 μl of ice-cold

immunoprecipitation buffer (300 mM NaCl, 50 mM Tris-HCl, pH 7.4, 1% Triton X-100, complete protease inhibitor mixture) by sonication. Lysates were cleared by centrifugation at 14,000 × *g* for 15 min. 50 μl of supernatant were saved as input fraction, and the remaining 450 μl were incubated with 20 μl of Protein G beads (GE Healthcare) and 2 μg of antibodies on a rocker at 4 °C for 1 h. After three washes with immunoprecipitation buffer, proteins were eluted with 40 μl of 2× SDS sample buffer. 10 μl of each sample were analyzed by SDS-PAGE followed by Western blotting using horseradish peroxidase–conjugated secondary antibodies and an ECL West Pico (Thermo Scientific) detection system. Both lysates and immunoprecipitated fractions were run on the same gel followed by taking different exposures reported on different panels to accommodate for differences in protein content and resulting immunoreactivity.

Data analysis and statistics

A minimum of three animals were used in each group throughout the study. For statistical analyses, data were analyzed from individual cells. Statistical analysis was performed using GraphPad Prism (Prism 6.0, GraphPad, San Diego, CA) and SPSS Statistics 25 software (IBM). Student's *t* test was used to compare means between two groups, and one-way or two-way ANOVA followed by Bonferroni post hoc test was used to determine significant differences among multiple groups. Repeated-measures ANOVA was used when a dependent variable was measured multiple times such as intrinsic excitability, barium-sensitive current, and forskolin-mediated Kv4.2 current inhibition. Statistical tests were performed two-sided. Differences were considered significant if p was <0.05. All data are expressed as means ± S.E.

Author contributions—C. S., C. O., and L. P. S. formal analysis; C. S., C. O., and L. P. S. investigation; C. S. and K. A. M. writing-original draft; C. O., L. P. S., and K. A. M. writing-review and editing; K. A. M. conceptualization; K. A. M. supervision; K. A. M. funding acquisition; K. A. M. project administration.

Acknowledgments—We thank Natalia Martemyanova for help with breeding and maintenance of mouse lines used in these experiments and members of the Martemyanov laboratory for critical feedback on the results and interpretations.

References

1. Radley, J. J., Rocher, A. B., Miller, M., Janssen, W. G., Liston, C., Hof, P. R., McEwen, B. S., and Morrison, J. H. (2006) Repeated stress induces dendritic spine loss in the rat medial prefrontal cortex. *Cereb. Cortex* **16,** 313–320 CrossRef Medline
2. Cook, S. C., and Wellman, C. L. (2004) Chronic stress alters dendritic morphology in rat medial prefrontal cortex. *J. Neurobiol.* **60,** 236–248 CrossRef Medline
3. Radley, J. J., and Morrison, J. H. (2005) Repeated stress and structural plasticity in the brain. *Ageing Res. Rev.* **4,** 271–287 CrossRef Medline
4. Wilber, A. A., Walker, A. G., Southwood, C. J., Farrell, M. R., Lin, G. L., Rebec, G. V., and Wellman, C. L. (2011) Chronic stress alters neural activity in medial prefrontal cortex during retrieval of extinction. *Neuroscience* **174,** 115–131 CrossRef Medline
5. Rosenkranz, J. A., Venheim, E. R., and Padival, M. (2010) Chronic stress causes amygdala hyperexcitability in rodents. *Biol. Psychiatry* **67,** 1128–1136 CrossRef Medline
6. Wallace, D. L., Han, M. H., Graham, D. L., Green, T. A., Vialou, V., Iñiguez, S. D., Cao, J. L., Kirk, A., Chakravarty, S., Kumar, A., Krishnan, V., Neve, R. L., Cooper, D. C., Bolaños, C. A., Barrot, M., *et al.* (2009) CREB regulation of nucleus accumbens excitability mediates social isolation-induced behavioral deficits. *Nat. Neurosci.* **12,** 200–209 CrossRef Medline
7. Wang, G. Q., Cen, C., Li, C., Cao, S., Wang, N., Zhou, Z., Liu, X. M., Xu, Y., Tian, N. X., Zhang, Y., Wang, J., Wang, L. P., and Wang, Y. (2015) Deactivation of excitatory neurons in the prelimbic cortex via Cdk5 promotes pain sensation and anxiety. *Nat. Commun.* **6,** 7660 CrossRef Medline
8. Papadopoulou, A., Siamatras, T., Delgado-Morales, R., Amin, N. D., Shukla, V., Zheng, Y. L., Pant, H. C., Almeida, O. F., and Kino, T. (2015) Acute and chronic stress differentially regulate cyclin-dependent kinase 5 in mouse brain: implications to glucocorticoid actions and major depression. *Transl. Psychiatry* **5,** e578 CrossRef Medline
9. Jett, J. D., Bulin, S. E., Hatherall, L. C., McCartney, C. M., and Morilak, D. A. (2017) Deficits in cognitive flexibility induced by chronic unpredictable stress are associated with impaired glutamate neurotransmission in the rat medial prefrontal cortex. *Neuroscience* **346,** 284–297 CrossRef Medline
10. Covington, H. E., 3rd, Lobo, M. K., Maze, I., Vialou, V., Hyman, J. M., Zaman, S., LaPlant, Q., Mouzon, E., Ghose, S., Tamminga, C. A., Neve, R. L., Deisseroth, K., and Nestler, E. J. (2010) Antidepressant effect of optogenetic stimulation of the medial prefrontal cortex. *J. Neurosci.* **30,** 16082–16090 CrossRef Medline
11. Koenigs, M., and Grafman, J. (2009) The functional neuroanatomy of depression: distinct roles for ventromedial and dorsolateral prefrontal cortex. *Behav. Brain Res.* **201,** 239–243 CrossRef Medline
12. van Harmelen, A. L., van Tol, M. J., Dalgleish, T., van der Wee, N. J., Veltman, D. J., Aleman, A., Spinhoven, P., Penninx, B. W., and Elzinga, B. M. (2014) Hypoactive medial prefrontal cortex functioning in adults reporting childhood emotional maltreatment. *Soc. Cogn. Affect. Neurosci.* **9,** 2026–2033 CrossRef Medline
13. Ongür, D., and Price, J. L. (2000) The organization of networks within the orbital and medial prefrontal cortex of rats, monkeys and humans. *Cereb. Cortex* **10,** 206–219 CrossRef Medline
14. Verwer, R. W., Meijer, R. J., Van Uum, H. F., and Witter, M. P. (1997) Collateral projections from the rat hippocampal formation to the lateral and medial prefrontal cortex. *Hippocampus* **7,** 397–402 CrossRef Medline
15. Zhang, B., Guo, F., Ma, Y., Song, Y., Lin, R., Shen, F. Y., Jin, G. Z., Li, Y., and Liu, Z. Q. (2017) Activation of D1R/PKA/mTOR signaling cascade in medial prefrontal cortex underlying the antidepressant effects of l-SPD. *Sci. Rep.* **7,** 3809 CrossRef Medline
16. Perrotti, L. I., Hadeishi, Y., Ulery, P. G., Barrot, M., Monteggia, L., Duman, R. S., and Nestler, E. J. (2004) Induction of ΔFosB in reward-related brain structures after chronic stress. *J. Neurosci.* **24,** 10594–10602 CrossRef Medline
17. Vialou, V., Bagot, R. C., Cahill, M. E., Ferguson, D., Robison, A. J., Dietz, D. M., Fallon, B., Mazei-Robison, M., Ku, S. M., Harrigan, E., Winstanley, C. A., Joshi, T., Feng, J., Berton, O., and Nestler, E. J. (2014) Prefrontal cortical circuit for depression- and anxiety-related behaviors mediated by cholecystokinin: role of ΔFosB. *J. Neurosci.* **34,** 3878–3887 CrossRef Medline
18. Vialou, V., Robison, A. J., Laplant, Q. C., Covington, H. E., 3rd, Dietz, D. M., Ohnishi, Y. N., Mouzon, E., Rush, A. J., 3rd, Watts, E. L., Wallace, D. L., Iñiguez, S. D., Ohnishi, Y. H., Steiner, M. A., Warren, B. L., Krishnan, V., *et al.* (2010) ΔFosB in brain reward circuits mediates resilience to stress and antidepressant responses. *Nat. Neurosci.* **13,** 745–752 CrossRef Medline
19. Shrestha, P., Mousa, A., and Heintz, N. (2015) Layer 2/3 pyramidal cells in the medial prefrontal cortex moderate stress induced depressive behaviors. *Elife* **4,** e08752 CrossRef Medline
20. Reiach, J. S., Li, P. P., Warsh, J. J., Kish, S. J., and Young, L. T. (1999) Reduced adenylyl cyclase immunolabeling and activity in postmortem temporal cortex of depressed suicide victims. *J. Affect. Disord.* **56,** 141–151 CrossRef Medline
21. Dwivedi, Y., Rizavi, H. S., Conley, R. R., Roberts, R. C., Tamminga, C. A., and Pandey, G. N. (2003) Altered gene expression of brain-derived neu-

rotrophic factor and receptor tyrosine kinase B in postmortem brain of suicide subjects. *Arch. Gen. Psychiatry* **60,** 804–815 CrossRef Medline
22. Fujita, M., Richards, E. M., Niciu, M. J., Ionescu, D. F., Zoghbi, S. S., Hong, J., Telu, S., Hines, C. S., Pike, V. W., Zarate, C. A., and Innis, R. B. (2017) cAMP signaling in brain is decreased in unmedicated depressed patients and increased by treatment with a selective serotonin reuptake inhibitor. *Mol. Psychiatry* **22,** 754–759 CrossRef Medline
23. Wray, N. H., Schappi, J. M., Singh, H., Senese, N. B., and Rasenick, M. M. (2018) NMDAR-independent, cAMP-dependent antidepressant actions of ketamine. *Mol. Psychiatry* CrossRef Medline
24. Donati, R. J., and Rasenick, M. M. (2003) G protein signaling and the molecular basis of antidepressant action. *Life Sci.* **73,** 1–17 CrossRef Medline
25. Zhong, P., Liu, X., Zhang, Z., Hu, Y., Liu, S. J., Lezama-Ruiz, M., Joksimovic, M., and Liu, Q. S. (2014) Cyclin-dependent kinase 5 in the ventral tegmental area regulates depression-related behaviors. *J. Neurosci.* **34,** 6352–6366 CrossRef Medline
26. Fan, Y., Kong, H., Ye, X., Ding, J., and Hu, G. (2016) ATP-sensitive potassium channels: uncovering novel targets for treating depression. *Brain Struct. Funct.* **221,** 3111–3122 CrossRef Medline
27. Chen, C., Wang, L., Rong, X., Wang, W., and Wang, X. (2015) Effects of fluoxetine on protein expression of potassium ion channels in the brain of chronic mild stress rats. *Acta Pharm. Sin. B* **5,** 55–61 CrossRef Medline
28. Hille, B. (1994) Modulation of ion-channel function by G-protein-coupled receptors. *Trends Neurosci.* **17,** 531–536 CrossRef Medline
29. den Boon, F. S., Chameau, P., Schaafsma-Zhao, Q., van Aken, W., Bari, M., Oddi, S., Kruse, C. G., Maccarrone, M., Wadman, W. J., and Werkman, T. R. (2012) Excitability of prefrontal cortical pyramidal neurons is modulated by activation of intracellular type-2 cannabinoid receptors. *Proc. Natl. Acad. Sci. U.S.A.* **109,** 3534–3539 CrossRef Medline
30. Golan, M., Schreiber, G., and Avissar, S. (2009) Antidepressants, beta-arrestins and GRKs: from regulation of signal desensitization to intracellular multifunctional adaptor functions. *Curr. Pharm. Des.* **15,** 1699–1708 CrossRef Medline
31. Stratinaki, M., Varidaki, A., Mitsi, V., Ghose, S., Magida, J., Dias, C., Russo, S. J., Vialou, V., Caldarone, B. J., Tamminga, C. A., Nestler, E. J., and Zachariou, V. (2013) Regulator of G protein signaling 4 [corrected] is a crucial modulator of antidepressant drug action in depression and neuropathic pain models. *Proc. Natl. Acad. Sci. U.S.A.* **110,** 8254–8259 CrossRef Medline
32. Ghanemi, A. (2015) Targeting G protein coupled receptor-related pathways as emerging molecular therapies. *Saudi Pharm. J.* **23,** 115–129 CrossRef Medline
33. Tomita, H., Ziegler, M. E., Kim, H. B., Evans, S. J., Choudary, P. V., Li, J. Z., Meng, F., Dai, M., Myers, R. M., Neal, C. R., Speed, T. P., Barchas, J. D., Schatzberg, A. F., Watson, S. J., Akil, H., *et al.* (2013) G protein-linked signaling pathways in bipolar and major depressive disorders. *Front. Genet.* **4,** 297 CrossRef Medline
34. Ehrlich, A. T., Maroteaux, G., Robe, A., Venteo, L., Nasseef, M. T., van Kempen, L. C., Mechawar, N., Turecki, G., Darcq, E., and Kieffer, B. L. (2018) Expression map of 78 brain-expressed mouse orphan GPCRs provides a translational resource for neuropsychiatric research. *Commun. Biol.* **1,** 102 CrossRef Medline
35. Sutton, L. P., Orlandi, C., Song, C., Oh, W. C., Muntean, B. S., Xie, K., Filippini, A., Xie, X., Satterfield, R., Yaeger, J. D. W., Renner, K. J., Young, S. M., Jr., Xu, B., Kwon, H., and Martemyanov, K. A. (2018) Orphan receptor GPR158 controls stress-induced depression. *Elife* **7,** e33273 CrossRef Medline
36. Orlandi, C., Xie, K., Masuho, I., Fajardo-Serrano, A., Lujan, R., and Martemyanov, K. A. (2015) Orphan receptor GPR158 is an allosteric modulator of RGS7 catalytic activity with an essential role in dictating its expression and localization in the brain. *J. Biol. Chem.* **290,** 13622–13639 CrossRef Medline
37. Orlandi, C., Sutton, L. P., Muntean, B. S., Song, C., and Martemyanov, K. A. (2019) Homeostatic cAMP regulation by the RGS7 complex controls depression-related behaviors. *Neuropsychopharmacology* **44,** 642–653 CrossRef Medline
38. Song, C., Ehlers, V. L., and Moyer, J. R., Jr. (2015) Trace fear conditioning differentially modulates intrinsic excitability of medial prefrontal cortex-basolateral complex of amygdala projection neurons in infralimbic and prelimbic cortices. *J. Neurosci.* **35,** 13511–13524 CrossRef Medline
39. Song, C., and Moyer, J. R. (2018) Layer- and subregion-specific differences in the neurophysiological properties of rat medial prefrontal cortex pyramidal neurons. *J. Neurophysiol.* **119,** 177–191 CrossRef Medline
40. Alagem, N., Dvir, M., and Reuveny, E. (2001) Mechanism of Ba^{2+} block of a mouse inwardly rectifying K^+ channel: differential contribution by two discrete residues. *J. Physiol.* **534,** 381–393 CrossRef Medline
41. Kehl, S. J., Fedida, D., and Wang, Z. (2013) External Ba^{2+} block of Kv4.2 channels is enhanced in the closed-inactivated state. *Am. J. Physiol. Cell Physiol.* **304,** C370–C381 CrossRef Medline
42. Yost, C. S. (1999) Potassium channels: basic aspects, functional roles, and medical significance. *Anesthesiology* **90,** 1186–1203 CrossRef Medline
43. Kim, J., Wei, D. S., and Hoffman, D. A. (2005) Kv4 potassium channel subunits control action potential repolarization and frequency-dependent broadening in rat hippocampal CA1 pyramidal neurones. *J. Physiol.* **569,** 41–57 CrossRef Medline
44. Carrasquillo, Y., Burkhalter, A., and Nerbonne, J. M. (2012) A-type K^+ channels encoded by Kv4.2, Kv4.3 and Kv1.4 differentially regulate intrinsic excitability of cortical pyramidal neurons. *J. Physiol.* **590,** 3877–3890 CrossRef Medline
45. Storm, J. F. (1990) Potassium currents in hippocampal pyramidal cells. *Prog. Brain Res.* **83,** 161–187 CrossRef Medline
46. Guan, D., Horton, L. R., Armstrong, W. E., and Foehring, R. C. (2011) Postnatal development of A-type and Kv1- and Kv2-mediated potassium channel currents in neocortical pyramidal neurons. *J. Neurophysiol.* **105,** 2976–2988 CrossRef Medline
47. Kim, J., Jung, S. C., Clemens, A. M., Petralia, R. S., and Hoffman, D. A. (2007) Regulation of dendritic excitability by activity-dependent trafficking of the A-type K^+ channel subunit Kv4.2 in hippocampal neurons. *Neuron* **54,** 933–947 CrossRef Medline
48. Marionneau, C., LeDuc, R. D., Rohrs, H. W., Link, A. J., Townsend, R. R., and Nerbonne, J. M. (2009) Proteomic analyses of native brain $K_V4.2$ channel complexes. *Channels* **3,** 284–294 CrossRef Medline
49. Marionneau, C., Townsend, R. R., and Nerbonne, J. M. (2011) Proteomic analysis highlights the molecular complexities of native Kv4 channel macromolecular complexes. *Semin. Cell Dev. Biol.* **22,** 145–152 CrossRef Medline
50. Anderson, A. E., Adams, J. P., Qian, Y., Cook, R. G., Pfaffinger, P. J., and Sweatt, J. D. (2000) Kv4.2 phosphorylation by cyclic AMP-dependent protein kinase. *J. Biol. Chem.* **275,** 5337–5346 CrossRef Medline
51. Hammond, R. S., Lin, L., Sidorov, M. S., Wikenheiser, A. M., and Hoffman, D. A. (2008) Protein kinase a mediates activity-dependent Kv4.2 channel trafficking. *J. Neurosci.* **28,** 7513–7519 CrossRef Medline
52. Roberson, E. D., English, J. D., Adams, J. P., Selcher, J. C., Kondratick, C., and Sweatt, J. D. (1999) The mitogen-activated protein kinase cascade couples PKA and PKC to cAMP response element binding protein phosphorylation in area CA1 of hippocampus. *J. Neurosci.* **19,** 4337–4348 CrossRef Medline
53. Schrader, L. A., Birnbaum, S. G., Nadin, B. M., Ren, Y., Bui, D., Anderson, A. E., and Sweatt, J. D. (2006) ERK/MAPK regulates the Kv4.2 potassium channel by direct phosphorylation of the pore-forming subunit. *Am. J. Physiol. Cell Physiol.* **290,** C852–C861 CrossRef Medline
54. McKlveen, J. M., Myers, B., and Herman, J. P. (2015) The medial prefrontal cortex: coordinator of autonomic, neuroendocrine and behavioural responses to stress. *J. Neuroendocrinol.* **27,** 446–456 CrossRef Medline
55. Arnsten, A. F. (2009) Stress signalling pathways that impair prefrontal cortex structure and function. *Nat. Rev. Neurosci.* **10,** 410–422 CrossRef Medline
56. Radley, J. J., Sisti, H. M., Hao, J., Rocher, A. B., McCall, T., Hof, P. R., McEwen, B. S., and Morrison, J. H. (2004) Chronic behavioral stress induces apical dendritic reorganization in pyramidal neurons of the medial prefrontal cortex. *Neuroscience* **125,** 1–6 CrossRef Medline
57. Holmes, A., and Wellman, C. L. (2009) Stress-induced prefrontal reorganization and executive dysfunction in rodents. *Neurosci. Biobehav. Rev.* **33,** 773–783 CrossRef Medline

58. Wang, M., Perova, Z., Arenkiel, B. R., and Li, B. (2014) Synaptic modifications in the medial prefrontal cortex in susceptibility and resilience to stress. *J. Neurosci.* **34,** 7485–7492 CrossRef Medline
59. Perova, Z., Delevich, K., and Li, B. (2015) Depression of excitatory synapses onto parvalbumin interneurons in the medial prefrontal cortex in susceptibility to stress. *J. Neurosci.* **35,** 3201–3206 CrossRef Medline
60. Witkowski, G., Rola, R., and Szulczyk, P. (2012) Effect of cyclic adenosine monophosphate on the G protein-dependent inward rectifier K^+-like channel current in medial prefrontal cortex pyramidal neurons. *J. Physiol. Pharmacol.* **63,** 457–462 Medline
61. Madison, D. V., and Nicoll, R. A. (1986) Cyclic adenosine 3′,5′-monophosphate mediates β-receptor actions of noradrenaline in rat hippocampal pyramidal cells. *J. Physiol.* **372,** 245–259 CrossRef Medline
62. Ostrovskaya, O., Xie, K., Masuho, I., Fajardo-Serrano, A., Lujan, R., Wickman, K., and Martemyanov, K. A. (2014) RGS7/Gβ5/R7BP complex regulates synaptic plasticity and memory by modulating hippocampal GABABR-GIRK signaling. *Elife* **3,** e02053 CrossRef Medline
63. Wainger, B. J., DeGennaro, M., Santoro, B., Siegelbaum, S. A., and Tibbs, G. R. (2001) Molecular mechanism of cAMP modulation of HCN pacemaker channels. *Nature* **411,** 805–810 CrossRef Medline
64. Wang, J., Chen, S., and Siegelbaum, S. A. (2001) Regulation of hyperpolarization-activated HCN channel gating and cAMP modulation due to interactions of COOH terminus and core transmembrane regions. *J. Gen. Physiol.* **118,** 237–250 CrossRef Medline
65. Kase, D., and Imoto, K. (2012) The role of HCN channels on membrane excitability in the nervous system. *J. Signal Transduct.* **2012,** 619747 CrossRef Medline
66. Huang, Z., Walker, M. C., and Shah, M. M. (2009) Loss of dendritic HCN1 subunits enhances cortical excitability and epileptogenesis. *J. Neurosci.* **29,** 10979–10988 CrossRef Medline
67. Magee, J. C. (1998) Dendritic hyperpolarization-activated currents modify the integrative properties of hippocampal CA1 pyramidal neurons. *J. Neurosci.* **18,** 7613–7624 CrossRef Medline
68. Surges, R., Brewster, A. L., Bender, R. A., Beck, H., Feuerstein, T. J., and Baram, T. Z. (2006) Regulated expression of HCN channels and cAMP levels shape the properties of the h current in developing rat hippocampus. *Eur. J. Neurosci.* **24,** 94–104 CrossRef Medline
69. Seo, H., Seol, M. J., and Lee, K. (2015) Differential expression of hyperpolarization-activated cyclic nucleotide-gated channel subunits during hippocampal development in the mouse. *Mol. Brain* **8,** 13 CrossRef Medline
70. Lörincz, A., Notomi, T., Tamás, G., Shigemoto, R., and Nusser, Z. (2002) Polarized and compartment-dependent distribution of HCN1 in pyramidal cell dendrites. *Nat. Neurosci.* **5,** 1185–1193 CrossRef Medline
71. Lockridge, A., Su, J., and Yuan, L. L. (2010) Abnormal 5-HT modulation of stress behaviors in the Kv4.2 knockout mouse. *Neuroscience* **170,** 1086–1097 CrossRef Medline
72. Kiselycznyk, C., Hoffman, D. A., and Holmes, A. (2012) Effects of genetic deletion of the Kv4.2 voltage-gated potassium channel on murine anxiety-, fear- and stress-related behaviors. *Biol. Mood Anxiety Disord.* **2,** 5 CrossRef Medline
73. Borsini, F., Volterra, G., and Meli, A. (1986) Does the behavioral "despair" test measure "despair"? *Physiol. Behav.* **38,** 385–386 CrossRef Medline
74. Cryan, J. F., Valentino, R. J., and Lucki, I. (2005) Assessing substrates underlying the behavioral effects of antidepressants using the modified rat forced swimming test. *Neurosci. Biobehav. Rev.* **29,** 547–569 CrossRef Medline
75. Hu, H. J., Carrasquillo, Y., Karim, F., Jung, W. E., Nerbonne, J. M., Schwarz, T. L., and Gereau, R. W., 4th (2006) The kv4.2 potassium channel subunit is required for pain plasticity. *Neuron* **50,** 89–100 CrossRef Medline
76. Cao, Y., Pahlberg, J., Sarria, I., Kamasawa, N., Sampath, A. P., and Martemyanov, K. A. (2012) Regulators of G protein signaling RGS7 and RGS11 determine the onset of the light response in ON bipolar neurons. *Proc. Natl. Acad. Sci. U.S.A.* **109,** 7905–7910 CrossRef Medline
77. Anderson, G. R., Lujan, R., Semenov, A., Pravetoni, M., Posokhova, E. N., Song, J. H., Uversky, V., Chen, C. K., Wickman, K., and Martemyanov, K. A. (2007) Expression and localization of RGS9–2/G 5/R7BP complex in vivo is set by dynamic control of its constitutive degradation by cellular cysteine proteases. *J. Neurosci.* **27,** 14117–14127 CrossRef Medline
78. Orlandi, C., Posokhova, E., Masuho, I., Ray, T. A., Hasan, N., Gregg, R. G., and Martemyanov, K. A. (2012) GPR158/179 regulate G protein signaling by controlling localization and activity of the RGS7 complexes. *J. Cell Biol.* **197,** 711–719 CrossRef Medline
79. Moyer, J. R., Jr., and Brown, T. H. (2007) Visually-guided patch-clamp recordings in brain slices, in *Advanced Techniques for Patch-Clamp Analysis* (Walz, W., ed) 2nd Ed., pp. 169–227, Humana Press, Totowa, NJ
80. Song, C., Anderson, G. R., Sutton, L. P., Dao, M., and Martemyanov, K. A. (2018) Selective role of RGS9-2 in regulating retrograde synaptic signaling of indirect pathway medium spiny neurons in dorsal striatum. *J. Neurosci.* **38,** 7120–7131 CrossRef Medline
81. Guan, D., Lee, J. C., Tkatch, T., Surmeier, D. J., Armstrong, W. E., and Foehring, R. C. (2006) Expression and biophysical properties of Kv1 channels in supragranular neocortical pyramidal neurones. *J. Physiol.* **571,** 371–389 CrossRef Medline
82. Guan, D., Tkatch, T., Surmeier, D. J., Armstrong, W. E., and Foehring, R. C. (2007) Kv2 subunits underlie slowly inactivating potassium current in rat neocortical pyramidal neurons. *J. Physiol.* **581,** 941–960 CrossRef Medline